8. R. Gao *et al*., *Org. Lett.* **3**, 3719 (2001).
9. Details of ^{31}P NMR spectra, phosphadioxirane decay kinetics, and epoxidation studies are available as supporting material on *Science* Online.
10. The upfield shift of the phosphorus signal indicates an unusually large R-P-R angle for a pentacoordinate phosphorus atom (R, aryl group), suggesting that the geometry around **2** is best described as distorted trigonal bipyramidal (*19*).
11. P. R. Bolduc, G. L. Goe, *J. Org. Chem.* **39**, 3178 (1974).
12. M. S. Reynolds, A. Butler, *Inorg. Chem.* **35**, 2378 (1996).
13. Coupling of the ^{17}O nucleus (I = 5/2) to the ^{31}P nucleus (I = 1/2) was not observed, because of the rapid quadrupolar relaxation, which leads to the very large signal width. The axial and equatorial oxygen of **2** could not be differentiated by this method, probably because pseudorotation is so fast that they become equivalent on the NMR time scale. Nahm *et al*. have determined by MP2 single-point calculations that the activation energy for pseudorotation of the dioxygen ligand in O_2PH_3 is only about 1 kcal/mol (*7*).
14. M. Von Itzstein, I. D. Jenkins, *J. Chem. Soc. Chem. Commun.* **164** (1983).
15. INTKIN is a noncommercial program developed by H. Schwarz at Brookhaven National Laboratory.
16. K. C. Eapen, C. Tamborski, *J. Fluorine Chem.* **15**, 239 (1980).
17. Time-resolved singlet oxygen luminescence quenching experiments are conducted by exciting a solution containing the sensitizer (tetraphenyl porphyrin or rose bengal) and varying amounts of substrate (quencher) with a short (a few nanoseconds) laser pulse and monitoring the $^1O_2$ decay at right angles.
18. Competition experiments show that no physical quenching occurred for phosphine **8**, because the rate of product formation was twice the rate of singlet oxygen removal, as one would expect if all of the $^1O_2$ was converted to product.
19. D. G. Gorenstein, in *Phosphorus-31 NMR Principles and Applications*, D. G. Gorenstein, Ed. (Academic Press, Orlando, FL, 1984), pp. 14–15.
20. Y. Zhao, K. N. Houk, personal communication.
21. Support by the NIH–National Institute of General Medical Sciences MBRS program (Award GM 08101) is gratefully acknowledged. Acknowledgment is also made to the Donors of The Petroleum Research Fund, administered by the American Chemical Society, for partial support of this research. J.C. was supported by the NIH Biomedical Post-Baccalaureate Research Program (Award GM 64104).

Supporting Online Material
www.sciencemag.org/cgi/content/full/302/5643/259/DC1
Materials and Methods
Figs. S1 to S3

14 July 2003; accepted 25 August 2003

Protein Conformational Dynamics Probed by Single-Molecule Electron Transfer

Haw Yang,[1]* Guobin Luo,[1] Pallop Karnchanaphanurach,[1] Tai-Man Louie,[2] Ivan Rech,[3] Sergio Cova,[3] Luying Xun,[2] X. Sunney Xie[1]†

Electron transfer is used as a probe for angstrom-scale structural changes in single protein molecules. In a flavin reductase, the fluorescence of flavin is quenched by a nearby tyrosine residue by means of photo-induced electron transfer. By probing the fluorescence lifetime of the single flavin on a photon-by-photon basis, we were able to observe the variation of flavin-tyrosine distance over time. We could then determine the potential of mean force between the flavin and the tyrosine, and a correlation analysis revealed conformational fluctuation at multiple time scales spanning from hundreds of microseconds to seconds. This phenomenon suggests the existence of multiple interconverting conformers related to the fluctuating catalytic reactivity.

The conformational dynamics of biomolecules is crucial to their biological functions, but these motions are usually spontaneous and unsynchronized and thus difficult to probe in ensemble-averaged experiments. Recent advances in room-temperature single-molecule fluorescence spectroscopy allow for real-time observations of conformational motions and chemical reactions on biologically relevant time scales (*1*–*4*). For example, by observing the enzymatic reaction of a single cholesterol oxidase molecule in real time, Lu *et al.* deduced that the slowly interconverting conformers exhibit different catalytic reactivities (*5*). Recently, van Oijen *et al.* found slow fluctuation in catalytic activity of single DNA exonuclease molecules (*6*).

These studies recorded the changing reactivity of an enzyme molecule but did not directly report the conformational motions of the enzyme. Measurements of fluorescence lifetimes are more informative than measurements of fluorescence intensities, because the lifetimes are sensitively dependent on protein conformations. Electron transfer (ET) reactions are highly distance-dependent and have been observed through the measurements of fluorescence lifetime for small single molecules (*7*). Here, we show that the dynamics of excited state ET reactions within an enzyme molecule can reveal the presence of different conformations as well as the time scale of their interconversion. Our ET approach is sensitive to subtle distance changes on the angstrom scale and is complementary to the widely adopted fluorescence resonance energy transfer (FRET) technique, which has been used for studies of single-molecule conformational dynamics on the nanometer scale (*4*, *8*).

To study protein dynamics without perturbation, we used a naturally fluorescent flavin enzyme. The weak fluorescence from a single flavin fluorophore in protein (the isoalloxazine of a flavin cofactor) required us to use sensitive detection techniques. Another challenge was the extraction of dynamical information hidden in the single-molecule time traces. Here, we show probing conformational dynamics with submillisecond time resolution and a broad range of time scales (*9*).

We studied a flavin-enzyme system, a flavin reductase (Fre) from *Escherichia coli* with a bound flavin, which is suggested to be involved in DNA synthesis by means of the activation of ribonucleotide reductase (*10*). Fre catalyzes the reduction of a flavin by a reduced form of nicotinamide adenine dinucleotide (NADH) through a hydride transfer reaction. The crystal structure of the 26-kD Fre has been solved both with and without riboflavin (*11*) (Fig. 1A).

Flavin mononucleotide (FMN) and flavin adenine dinucleotide (FAD) are two typical flavin cofactors of Fre. The fluorescent isoalloxazine of flavins (Fig. 1A, yellow) serves as an ideal probe for conformational dynamics (*12*). Free isoalloxazine such as that of FMN (Fig. 1B, molecular structure) in a pH 7 buffer exhibits a monoexponential fluorescence decay with a 4.6-ns lifetime when excited at 440 nm in an ensemble-averaged experiment (Fig. 1B, green curve). In contrast, the decay of Fre-bound flavins is much faster and is multiexponential. For example, the fluorescence lifetime decay of the wild-type Fre/FMN complex (Fig. 1B, blue curve) can be best fitted with four exponential decays: 0.008 ns [19 weight (wt) %], 0.050 ns (39 wt %), 0.25 ns (39 wt %), and 4.5 ns (3.6 wt %) (*13*). However, the ensemble-averaged measurements in Fig. 1 cannot determine whether the multiexponential kinetics arise from static heterogeneity (in which the molecules are statically different) or dynamic fluctuations (in which a single molecule changes with time).

[1]Department of Chemistry and Chemical Biology, Harvard University, Cambridge, MA 02138, USA. [2]School of Molecular Biosciences, Washington State University, Pullman, WA 99164, USA. [3]Department of Electronics and Information, Politecnico di Milano and Centro Elettronica Quantistica e Strumentazione Elettronica Council of National Research, 20133 Milano, Italy.

*Present address: Department of Chemistry, University of California, Berkeley, CA 94720, USA.
†To whom correspondence should be addressed. E-mail: xie@chemistry.harvard.edu

Downloaded from http://science.sciencemag.org/ on January 4, 2018

The fast fluorescence decay of isoalloxazine inside protein has been attributed to the quenching of the excited state by ET from nearby residues such as Trp or Tyr (Y) (*12*, *14*, *15*). According to the crystal structure, there are three tyrosines—Tyr^{35}, Tyr^{72}, and Tyr^{116}—near the isoalloxazine, with edge-to-edge distances to the isoalloxazine of 4.5, 9.6, and 7.0 Å, respectively. To identify the residues responsible for the quenching of flavin fluorescence, we replaced the three tyrosines individually with a serine (S) and generated three mutants—Y35S, Y72S, and Y116S—by site-directed mutagenesis. The fluorescence decays of the two mutant complexes Y72S/FMN (pink curve) and Y116S/FMN (orange curve) are similar to that of the wild-type Fre/FMN (Fig. 1B). A drastic increase of fluorescence lifetime, however, was observed for the Y35S/FMN complex (red curve). Therefore, we attribute the quenching of isoalloxazine fluorescence in wild-type Fre/FMN to ET from primarily the closest Tyr^{35} (Fig. 1A, red) to the isoalloxazine. The reverse ET is expected to complete rapidly, returning isoalloxazine and Tyr^{35} to their original states for repetitive excitation (*15*).

The other flavin substrate, FAD (Fig. 1C, molecular structure), binds Fre tightly in the absence of NADH with a dissociation constant K_d of ~29 nM, compared with the loose binding of Fre/FMN, which has a K_d of ~1.5 μM (*16*). We chose to do single-molecule measurements on the wild-type Fre/FAD complex for its stability. By means of the molecular dynamics (MD) simulations that were based on the Fre/riboflavin structure, we obtained a representative configuration of the Fre/FAD complex (Fig. 1A) (*16*). The MD configurations indicate that the isoalloxazine of FAD is enclosed in the flavin-binding pocket with several hydrogen bonds, whereas the adenine (Fig. 1A, gray) of FAD extends to the exterior of the protein. On average, the adenine tail forms two additional hydrogen bonds with Fre, which explains the higher affinity of FAD to Fre over FMN (*16*).

The isoalloxazine fluorescence of unbound FAD is partially quenched by its flexible adenine tail in aqueous solution (evident from the faster decay of the green curve in Fig. 1C than that in Fig. 1B). Based on the extended structure of FAD in the protein, quenching by adenine is negligible in the protein. Indeed, the multiexponential fluorescence decays of the wild-type or mutant Fre/FAD (Fig. 1C) are similar to those of Fre/FMN complexes. The fluorescence decay of the wild-type Fre/FAD (Fig. 1C, blue curve) can be best fitted with four exponential decays: 0.028 ns (25 wt %), 0.20 ns (52.1 wt %), 0.46 ns (21.5 wt %), and 3.3 ns (1.2 wt %).

The fitting of the ensemble data by no means reflects the true distribution of fluorescence lifetime. Assuming the population decay is from a single electronic excited state in our system, the (fluctuating) fluorescence lifetime $\gamma^{-1}(t)$ can be expressed as: $\gamma^{-1}(t) = [\gamma_0 + k_{ET}(t)]^{-1} \approx k_{ET}^{-1}(t)$, where γ_0 is the fluorescence decay rate in the absence of the quencher(s), and k_{ET} is the ET rate. We seek to characterize the distribution and fluctuation of k_{ET},

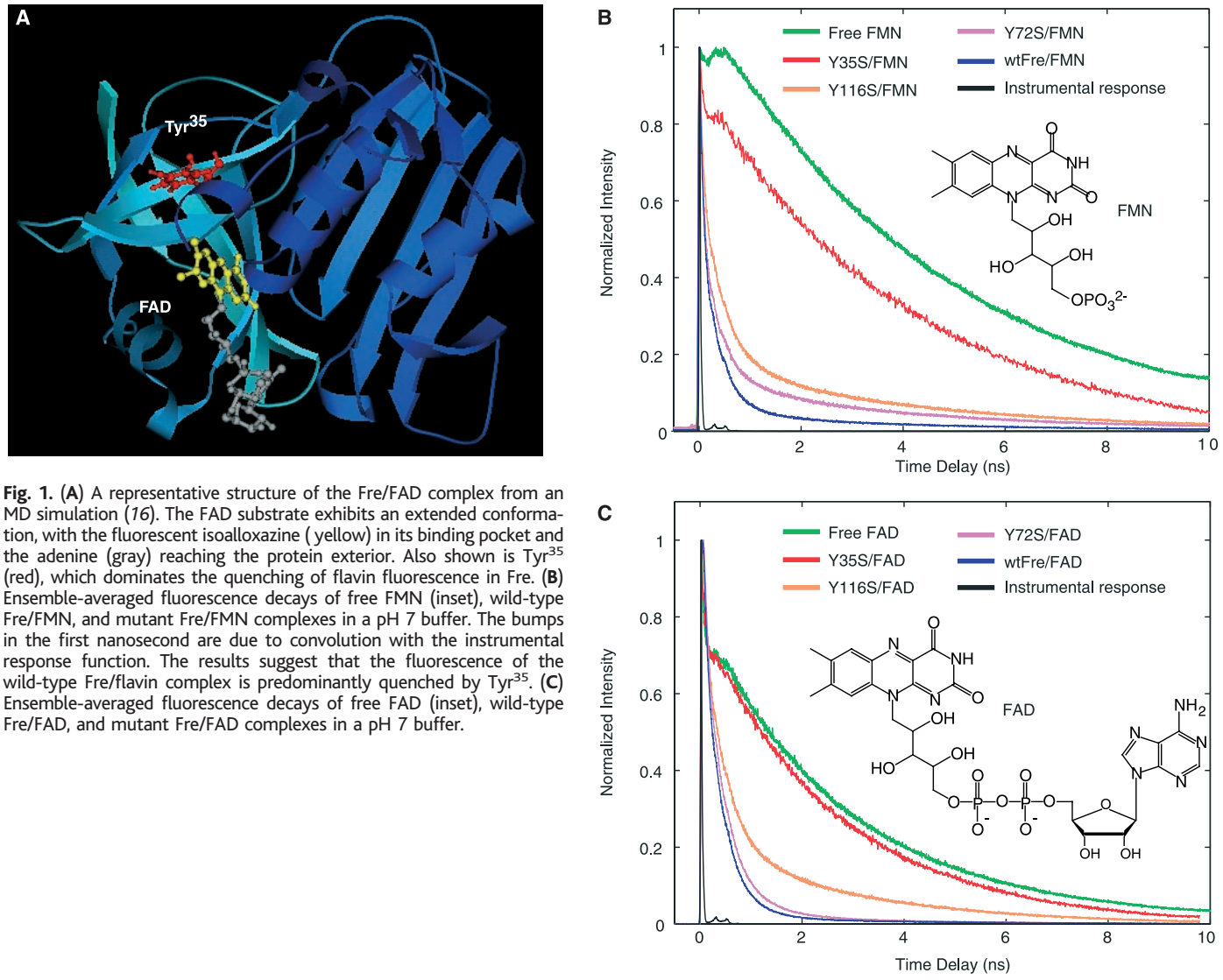

Fig. 1. (**A**) A representative structure of the Fre/FAD complex from an MD simulation (*16*). The FAD substrate exhibits an extended conformation, with the fluorescent isoalloxazine (yellow) in its binding pocket and the adenine (gray) reaching the protein exterior. Also shown is Tyr^{35} (red), which dominates the quenching of flavin fluorescence in Fre. (**B**) Ensemble-averaged fluorescence decays of free FMN (inset), wild-type Fre/FMN, and mutant Fre/FMN complexes in a pH 7 buffer. The bumps in the first nanosecond are due to convolution with the instrumental response function. The results suggest that the fluorescence of the wild-type Fre/flavin complex is predominantly quenched by Tyr^{35}. (**C**) Ensemble-averaged fluorescence decays of free FAD (inset), wild-type Fre/FAD, and mutant Fre/FAD complexes in a pH 7 buffer.

Downloaded from http://science.sciencemag.org/ on January 4, 2018

the information hidden in ensemble results but extractable from a single-molecule experiment.

The Fre/FAD complex is tethered to the quartz surface by a biotin-streptavidin linkage (*13*). Special care was taken to avoid perturbations of the protein by the quartz surface (*17*). Commercially available detectors do not provide the combination of high–photon timing resolution, low–dark counting rate, and high–quantum detection efficiency. A single-photon timing module (SPTM) has been designed and built based on the single-photon avalanche diode (SPAD) devices developed by Cova *et al.* (*18*, *19*).

Early single-molecule lifetime measurements used the standard time-correlated photon counting method (*7*, *20*, *21*) to record histograms of the delay times of fluorescence photons with respect to the excitation pulses. Figure 2 is such a histogram for a single wild-type Fre/FAD complex immobilized on the quartz surface. The multiexponential single-molecule decay, similar to the ensemble-averaged decay (Fig. 1C), indicates fluctuations of fluorescence lifetime at a time scale longer than γ^{-1}. Similar multiexponential decays of single biomolecules have also been reported (*22*, *23*), in contrast to the mono-exponential decays of isolated single-dye molecules (*7*, *20*, *21*). However, the time-scrambled histograms provide no information about the dynamics of lifetime fluctuation, which can be obtained from single-molecule time traces.

Instead of acquiring only the histogram, for each detected fluorescence photon with index p, we recorded both the delay time with respect to its excitation pulse, τ_p, and the chronological arrival time, t_p (*9*, *24*) (Fig. 3A). Figure 3B shows part of the time trace of τ_p for the same complex in Fig. 2. If the γ^{-1} does not fluctuate, τ_p is stochastic and has a single exponential distribution with the mean of γ^{-1}. The fluctuating γ^{-1} results in the multiexponential decay of the τ_p histogram in Fig. 2 for all the photons in the entire time trace.

To evaluate how γ^{-1}changes with time, the conventional method is to bin many photons for an average γ^{-1}. For example, Fig. 3C shows part of the time trace of γ^{-1} by binning every 100 photons, in which large fluctuation of γ^{-1} is indeed evident. With the mean fluorescence count rate of 500 counts/s in our experiment, the time window corresponds to a mean of 200 ms. We used the maximum likelihood estimation (MLE) to determine γ^{-1} (*13*, *25*). It has been shown that 100 detected photons are sufficient to determine the single exponential decay constant by MLE. However, the binning limits the time resolution of dynamical changes; therefore, fluctuations within the time bin are averaged out.

The dynamics of fluctuation can be characterized by the correlation functions of γ^{-1} fluctuation, in particular, the autocorrelation function, $C(t) = \langle \delta\gamma^{-1}(t)\delta\gamma^{-1}(0)\rangle$, where $\delta\gamma^{-1}(t) = \gamma^{-1}(t) - \langle\gamma^{-1}\rangle$ and the brackets denote averaging over time. If there is no fluctuation of γ^{-1}, then $C(t) = 0$. When there are two interconverting states with different lifetimes, $C(t)$ is a single exponential decay with a decay constant equal to the sum of the forward and backward conversion rate constants (*9*). Multiple conformational states normally result in multiexponential decay $C(t)$, characterizing the time scales of γ^{-1} fluctuations, with $C(0)$ being the variance of γ^{-1}. $C(t)$ can be calculated from the time trace of γ^{-1} in Fig. 3C, although with a poor time resolution.

Accurate knowledge of $\gamma^{-1}(t)$ from long time binning is not required to determine $C(t)$, which itself is a statistically averaged property. The time resolution of $C(t)$ can be significantly improved if $C(t)$ is calculated on a photon-by-photon basis (*9*, *13*). We obtained a time resolution of $C(t)$ comparable to the reciprocal of the average count rate. The time resolution in principle can approach that of the ever-increasing length of MD simulation trajectories (*26*), which portends direct comparison between single-molecule experiments with MD simulations in the future. Consequently, our approach permits measurements of $C(t)$ on a broad range of time scales for the given time-trace lengths, limited by photobleaching. In our analysis, background photons will not contribute to $C(t > 0)$, because they are not correlated with fluorescence photons from the single molecule.

Figure 4 shows the $C(t)$ of a wild-type Fre/FAD complex, with fluctuation occurring at a broad range of time scales, from hundreds of microseconds to tens of seconds. This information was not available from previous ensemble-averaged experiments. The green dashed line in Fig. 4 is a fit with a stretched exponential, $\exp[-(t/\tau_0)^b]$, where $b = 0.30$ and $\tau_0 = 54$ ms. The stretched exponential is simply a phenom-

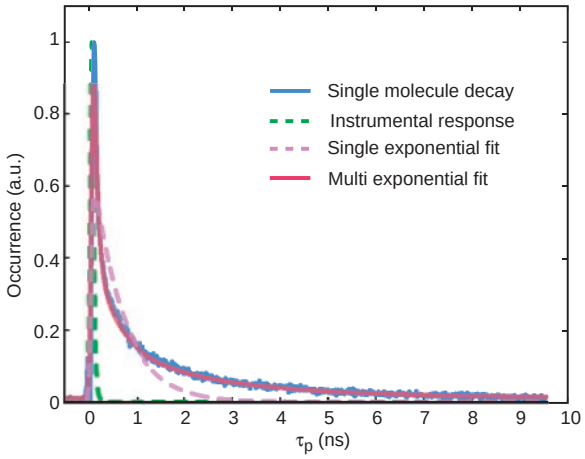

Fig. 2. Multiexponential fluorescence decay of a single wild-type Fre/FAD complex [best fitted with lifetime decay constants of 62 ps (77.3 wt %), 264 ps (14.3 wt %), and 2.26 ns (8.6 wt %)]. Also shown is the instrumental response function (with 60-ps full width at half maximum) and a poor fit with a monoexponential decay. a.u., arbitrary units.

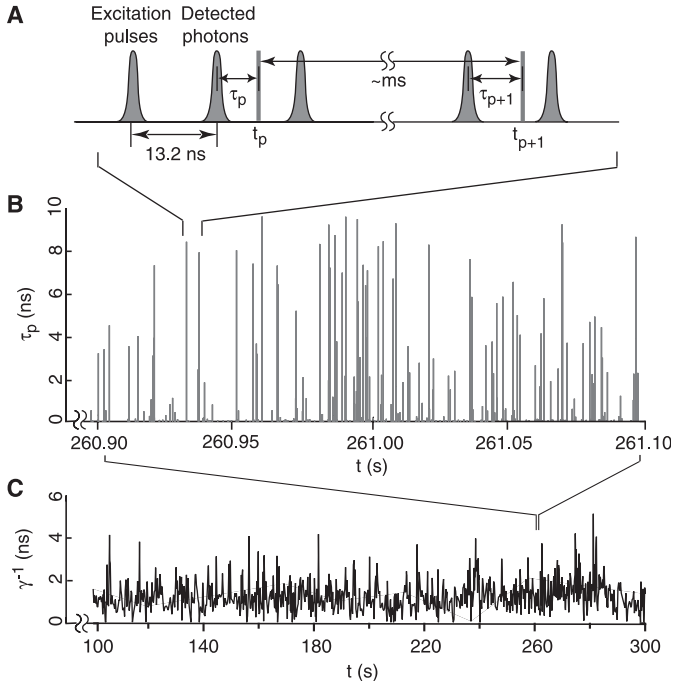

Fig. 3. (**A**) Schematic of a train of laser excitation pulses (bell shaped) and detected fluorescence photons (bars). For each detected photon, the delay time with respect to the excitation pulse τ_p and the chronological arrival t_p are recorded. (**B**) Part of the time trace of the fluorescence photon delay time of the same wild-type Fre/FAD complex as in Fig. 2. (**C**) Part of the time trace of the fluorescence lifetime of the same wild-type Fre/FAD complex as in (B) obtained by the MLE fitting of every 100 detected photons.

Downloaded from http://science.sciencemag.org/ on January 4, 2018

enological fit that conveniently describes dynamics spanning decades of time scales with only two adjustable parameters rather than multiple exponentials. Fluorophores that exhibited single exponential fluorescence decay showed zero $C(t > 0)$ (fig. S5). For every wild-type Fre/FAD complex that emits a sufficient number of photons (>100,000) to give visible correlation before photobleaching, we observed similar stretched exponential $C(t)$ with b varying from 0.17 to 0.31. We did not observe noticeable power dependence of $C(t)$ in the excitation power range from 0.5 to 3 μW at the sample (*13*). Had the fluctuations been photoinduced, $C(t)$ would have decayed faster at higher excitation powers, suggesting that the lifetime fluctuations are in fact spontaneous.

We next discuss the origin of $k_{ET}(t)$ fluctuations. On the basis of Fermi's golden rule, the nonadiabatic ET rate is $k_{ET} = (4\pi^2/h)V^2F$, where h is Planck's constant, V is the electronic coupling between the two diabatic states (DA and D^+A^-), and F is the Franck-Condon weighted density of states (*27*, *28*). We then considered whether the k_{ET} variation arises from the fluctuation of V or F.

At room temperatures, F takes a simple Arrhenius form (*27*, *28*), $k_{ET} = (4\pi^2/h)V^2(4\pi k_BT\lambda)^{-1/2}\exp[-(\Delta G + \lambda)^2/4\lambda k_BT]$, where k_B is the Boltzmann constant, T is temperature in kelvin, ΔG is the free energy difference between DA and D^+A^-, and λ is the reorganization energy. Thermal fluctuation of ΔG could lead to fluctuation of k_{ET} as in photosynthetic reaction centers (*29*, *30*). For the electronically excited FAD/tyrosine system, the k_{ET} is close to the maximum rate at which $-\Delta G \sim \lambda = 28 \sim 40k_BT$ (0.7 to 1.0 eV) (*14*). Under this activationless condition, k_{ET} is relatively insensitive to thermal fluctuations in ΔG. If ΔG variation (denoted as $\Delta\Delta G$) is the sole source of k_{ET} fluctuation, the large amplitude of the observed k_{ET} fluctuation (a difference of more than one order of magnitude, with time constants ranging from 30 ps to 3 ns) would result from an unphysically high $\Delta\Delta G \approx 16 \sim 20k_BT$.

However, the electronic coupling V exhibits an exponential dependence on the edge-to-edge distance R between D and A such that $k_{ET}(t) = k^0_{ET}\exp[-\beta R(t)]$, where β has been experimentally determined to be 1.0 to 1.4 $Å^{-1}$ for proteins (*31*, *32*). Distribution of ET rate originating from a (frozen) distribution of donor-acceptor distances was previously observed for photosynthetic reaction centers (*33*). V is also dependent on the relative orientations of D and A (*34*). Typically, however, the torsional angles of Tyr residues in the protein interior are confined to a narrow range (*35*). Because of the exponential distance dependence, R fluctuation has a much stronger effect on the ET rate than the effects of the driving force and orientation. We thus attribute the large lifetime fluctuations (30 ps to ~3 ns) primarily to R fluctuation.

We next determined the distribution of the isoalloxazine-Tyr^{35} distance, R. First, we obtained a distribution of γ^{-1} from the 100-photon binned time trace of γ^{-1} (Fig. 3C). The distribution is coarse-grained because the fast fluctuation within the time bin is averaged out. The corresponding coarse-grained lifetime probability density $P(\gamma^{-1})$ can be calculated (Fig. 5A). $P(\gamma^{-1})$ is converted to the probability density $P(R)$ assuming $\beta = 1.4\ Å^{-1}$ (Fig. 5B). Finally, the potential of mean force for the isoalloxazine-Tyr^{35} pair is obtained by taking the logarithm of $P(R)$: $V(R) = -k_BT\ln[P(R)]$. $V(R)$ can be approximated by a harmonic potential within the thermally attainable region (Fig. 5C) (*13*). The best fit of $P(\gamma^{-1})$ (*13*) with $V_0(R) = k_BT(R - R_0)^2/2\theta$ (Fig. 5C, dashed line) gives the variance of R, $\theta = 0.19\ Å^2$. θ compares favorably with the crystal-structure data, which gives average atomic-mean-square displacements of 0.10 and 0.25 $Å^2$ for the isoalloxazine and Tyr^{35}, respectively. This agreement further corroborates our assignment of k_{ET} fluctuation to primarily R fluctuation.

The potential of mean force $V(R)$ is a time-averaged function that does not contain dynamical information. To gain an understanding of the observed dynamics, we first modeled R fluctuation as a fictitious particle undergoing Brownian diffusion on the potential $V_0(R)$ and obtained the autocorrelation function $C_B(t) = (k^0_{ET})^{-2}\exp(2\beta R_0 + \beta^2\theta)[-1 + \exp(\beta^2\theta e^{-\eta t})]$ where η is a drift coefficient (*9*). However, $C_B(t)$ (Fig. 4, pink dashed line) does not fit the measured $C(t)$ (Fig. 4). The Brownian diffusion model is inadequate because it implies one characteristic trapping time (associated with η) at a particular R, which does not hold for complex systems like proteins (*36*, *37*). The trapping time, τ, at a particular R, might assume a power-

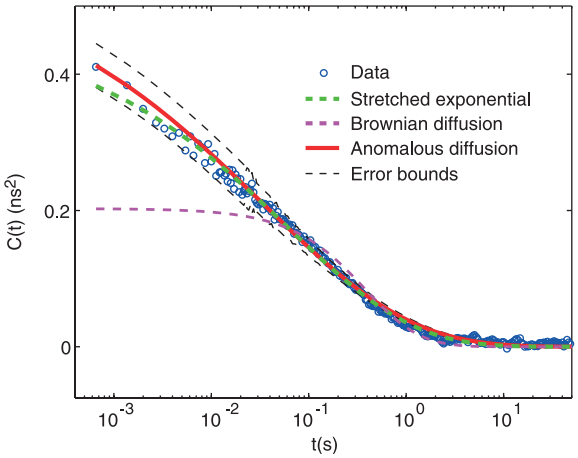

Fig. 4. Autocorrelation function of fluorescence lifetime fluctuation of the same wild-type Fre/FAD complex as in Figs. 2 and 3, plotted in linear logarithmic scale in time. Also shown are good fits with a stretched exponential and the anomalous diffusion model and a poor fit with the Brownian diffusion model. The $C(t)$ unravels protein conformational fluctuation spanning a broad range of time scales.

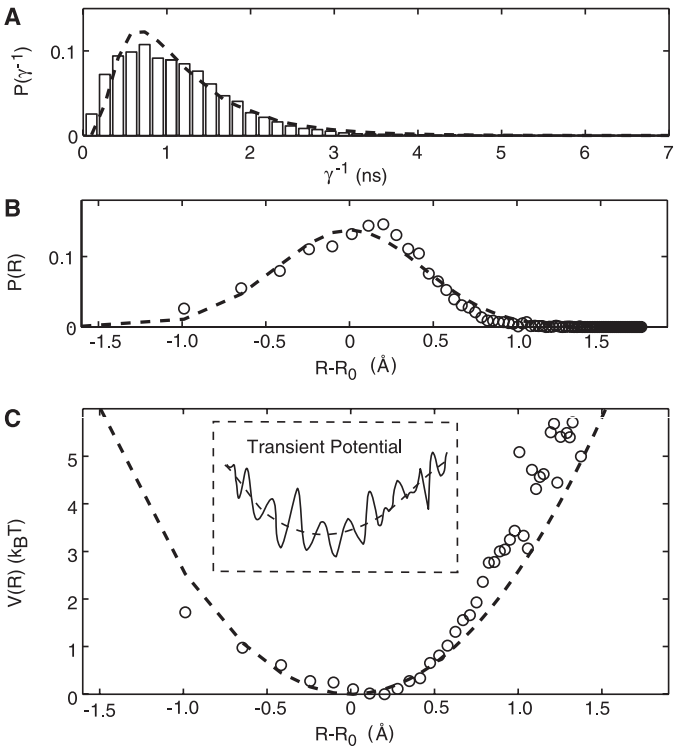

Fig. 5. (**A**) Distribution of fluorescence lifetimes obtained from the time trace in Fig. 2D. (**B**) Distribution of the FAD-Tyr^{35} edge-to-edge distance derived from (A). (**C**) Potential of mean force calculated from (B). The dashed lines in (A), (B), and (C) are distributions according to the fit to a harmonic potential of mean force around R_0 and with variance $\theta = 0.19\ Å^2$. (Inset) A sketch of a rugged "transient" potential resulting from the short-time projection of 3D motions of the protein to the experimentally accessible R coordinate.

Downloaded from http://science.sciencemag.org/ on January 4, 2018

law distribution, $1/\tau^{\alpha+1}$ ($0 < \alpha < 1$), which has no finite mean (*38*). This situation is referred to as the subdiffusion regime of anomalous diffusion. Subdiffusion in a potential can be described by the fractional Fokker-Planck equation recently developed by Klafter and co-workers (*38*). Using $V_0(R)$ as the potential, we obtained the correlation function (*9*)

$$C_A(t) = (k_{ET}^0)^{-2} \exp(2\beta R_0 + \beta^2\theta)$$
$$(\exp\{\beta^2\theta \exp[-\eta_\alpha t^\alpha/\Gamma(1+\alpha)]\} - 1)$$

where η_α is the generalized drift coefficient and $\Gamma(z) = \int_0^\infty y^{z-1}e^{-y}dy$. $C_A(t)$ (Fig. 4, red solid line) fits well with the measured $C(t)$, with $\alpha = 0.31$ and $\eta_\alpha = 2.19\ s^{-\alpha}$.

The physical picture behind $C_A(t)$ can be understood as follows: The multidimensional energy landscape of the entire protein has many local minima, each corresponding to a conformational state. The conformational states have vastly different trapping times because the free energy barrier heights for the interconversion among them are broadly distributed. Projection of the time-varying 3D structure of the protein to the experimentally accessible R coordinate results in a broad (power-law) distribution of trapping time at a particular R. Such a projection of 3D motion to the R dimension within a short period of time gives rise to a rugged "transient" potential (Fig. 5C, inset). With its long time average being the smoothed $V(R)$, the rugged potential with fluctuating free energy barriers results in the subdiffusion and the stretched exponential $C(t)$.

The picture of rugged energy landscape has been advocated by Frauenfelder based on photodissociation experiments with liganded hemeproteins (*39*). Reminiscent of glassy systems (*40*), ligand recombination kinetics at low temperatures exhibited dispersed kinetics because of a frozen distribution of conformations, the interconversion among which occurs at elevated temperatures. Even at room temperature, stretched exponential relaxation of protein conformations has been observed (*41*). The ensemble-averaged experiments, however, could hardly distinguish dynamical fluctuation and static heterogeneity, nor could they extract the interconversion dynamics. It is important to stress that our single-molecule experiments directly measure the equilibrium fluctuation rather than nonequilibrium relaxation as in the previous experiments, and they provide a quantitative measure of the protein conformational memory at room temperature. A dynamic entity, an enzyme exhibits different catalytic activity (*5*, *6*) because of its fluctuating conformations.

References and Notes

1. S. M. Nie, R. N. Zare, *Annu. Rev. Biophys. Biomol. Struct.* **26**, 567 (1997).
2. X. S. Xie, J. K. Trautman, *Annu. Rev. Phys. Chem.* **49**, 441 (1998).
3. W. E. Moerner, M. Orrit, *Science* **283**, 1670 (1999).
4. S. Weiss, *Science* **283**, 1676 (1999).
5. H. P. Lu, L.-Y. Xun, X. S. Xie, *Science* **282**, 1877 (1998).
6. A. M. van Oijen *et al.*, *Science* **301**, 1235 (2003).
7. H. P. Lu, X. S. Xie, *J. Phys. Chem. B* **101**, 2753 (1997).
8. X. W. Zhuang *et al.*, *Science* **288**, 2048 (2000).
9. H. Yang, X. S. Xie, *J. Chem. Phys.* **117**, 10965 (2002).
10. M. Fontecave, R. Eliasson, P. Reichard, *J. Biol. Chem.* **262**, 12325 (1987).
11. M. Ingelman, S. Ramaswamy, V. Niviére, M. Fontecave, H. Eklund, *Biochemistry* **38**, 7040 (1999).
12. P. A. W. van den Berg, A. J. W. G. Visser, in *New Trends in Fluorescence Spectroscopy: Applications to Chemical and Life Sciences*, B. Valeur, J.-C. Brochon, Eds. (Springer, New York, 2001), pp. 457–485.
13. Materials and methods are available as supporting material on *Science* Online.
14. N. Mataga *et al.*, *J. Phys. Chem. B* **104**, 10667 (2000).
15. D. Zhong, A. H. Zewail, *Proc. Natl. Acad. Sci. U.S.A.* **98**, 11867 (2001).
16. T. Louie, H. Yang, P. Karnchanaphanurach, X. S. Xie, L.-Y. Xun, *J. Biol. Chem.* **277**, 39450 (2002).
17. To verify that the surface tethering introduces no complications, we also immobilized the Fre/FAD complex in 1% agarose gel between two cover slips with the method described in (*5*). We observed the same lifetime fluctuation of single Fre/FAD complexes tethered on quartz surface as in the agarose gel, although the agarose gel introduced a weak fluorescence background.
18. S. Cova, A. Laciata, M. Ghioni, G. Ripamonti, T. A. Louis, *Rev. Sci. Instrum.* **60**, 1104 (1989).
19. S. Cova, M. Ghioni, A. Lacaita, S. Samori, F. Zappa, *Appl. Optics* **35**, 1956 (1996).
20. X. S. Xie, R. C. Dunn, *Science* **265**, 361 (1994).
21. W. P. Ambrose, P. M. Goodwin, J. C. Martin, R. A. Keller, *Science* **265**, 364 (1994).
22. L. Edman, U. Mets, R. Rigler, *Proc. Natl. Acad. Sci. U.S.A.* **93**, 6710 (1996).
23. Y.-W. Jia *et al.*, *Proc. Natl. Acad. Sci. U.S.A.* **94**, 7932 (1997).
24. C. Eggeling, J. R. Fries, L. Brand, R. Günter, C. A. M. Seidel, *Proc. Natl. Acad. Sci. U.S.A.* **95**, 1556 (1998).
25. M. Köllner, J. Wolfrum, *Chem. Phys. Lett.* **200**, 199 (1992).
26. Y. Duan, P. A. Kollman, *Science* **282**, 740 (1998).
27. R. A. Marcus, N. Sutin, *Biochim. Biophys. Acta* **811**, 265 (1985).
28. J. Jortner, M. Bixon, Eds., *Electron Transfer—From Isolated Molecules to Biomolecules* (Wiley, New York, 1999), vol. 106.
29. M. Marchi, J. N. Gehlen, D. Chandler, M. Newton, *J. Am. Chem. Soc.* **115**, 4178 (1993).
30. J. N. Gehlen, M. Marchi, D. Chandler, *Science* **263**, 499 (1994).
31. C. C. Moser, J. M. Keske, K. Warncke, R. S. Farid, P. L. Dutton, *Nature* **355**, 796 (1992).
32. H. B. Gray, J. R. Winkler, *Annu. Rev. Biochem.* **65**, 537 (1996).
33. D. Kleinfeld, M. Y. Okamura, G. Feher, *Biochemistry* **23**, 5780 (1984).
34. P. Siders, R. J. Cave, R. A. Marcus, *J. Chem. Phys.* **81**, 5613 (1984).
35. J. A. Mccammon, P. G. Wolynes, M. Karplus, *Biochemistry* **18**, 927 (1979).
36. J.-P. Bouchaud, A. Georges, *Phys. Rep. Rev. Sec. Phys. Lett.* **195**, 12 (1990).
37. R. Metzler, J. Klafter, *Phys. Rep. Rev. Sec. Phys. Lett.* **339**, 1 (2000).
38. R. Metzler, E. Barkai, J. Klafter, *Phys. Rev. Lett.* **82**, 3563 (1999).
39. H. Frauenfelder, S. G. Sligar, P. G. Wolynes, *Science* **254**, 1598 (1991).
40. C. A. Angell, *Science* **267**, 1924 (1995).
41. T. A. Jackson, M. H. Lim, P. A. Anfinrud, *Chem. Phys.* **180**, 131 (1994).

42. Supported by NIH (R01GM61577-01, single-molecule biophysics) and in part by the Natural and Accelerated Bioremediation Research project of the Offices of Sciences, U.S. Department of Energy (DE-FG02-00ER62891, flavin enzymology). We thank R. A. Marcus, Y. Klafter, M. Karplus, D. Reichman, M. Okamura, S. G. Boxer, and I. Andricioaei for helpful discussions and V. Niviére for providing the protein coordinates used in MD simulation (Fig. 1A).

Supporting Online Material

www.sciencemag.org/cgi/content/full/302/5643/262/DC1
Materials and Methods
Figs. S1 to S6
References

16 May 2003; accepted 25 August 2003

Periodic Mesoporous Organosilicas Containing Interconnected $[Si(CH_2)]_3$ Rings

Kai Landskron,[1] Benjamin D. Hatton,[1,2] Doug D. Perovic,[2] Geoffrey A. Ozin*[1]

A periodic mesoporous organosilica composed of interconnected three-ring $[Si(CH_2)]_3$ units built of three $SiO_2(CH_2)_2$ tetrahedral subunits is reported. It represents the archetype of a previously unknown class of nanocomposite materials in which two bridging organic groups are bound to each silicon atom. It can be obtained with powder and oriented film morphologies. The nanocomposite is self-assembled from the cyclic three-ring silsesquioxane $[(EtO)_2Si(CH_2)]_3$ precursor and a surfactant mesophase to give a well-ordered mesoporous framework. Low dielectric constants and good mechanical stability of the films were measured, making this material interesting for microelectronic applications. Methylene group reactivity of the three-ring precursor provides entry to a family of nanocomposites, exemplified by the synthesis and self-assembly of $[(EtO)_2Si(CHR)][(EtO)_2Si(CH_2)]_2$ (where R indicates iodine, bromine, or an ethyl group).

Materials with well-defined pores belong to the most interesting classes of compounds, because they can be developed into organic-inorganic nanocomposites with unique catalytic, sensor, optical, magnetic, or electrical properties, whereby the organic functionalization of an inorganic porous host can play an important role (*1*). An exciting approach to organic-inorganic nanocomposites takes lessons from the synthesis of periodic mesoporous silica MCM41, where an organic mesophase is replicated in silica with the use of

Downloaded from http://science.sciencemag.org/ on January 4, 2018

Science

Protein Conformational Dynamics Probed by Single-Molecule Electron Transfer

Haw Yang, Guobin Luo, Pallop Karnchanaphanurach, Tai-Man Louie, Ivan Rech, Sergio Cova, Luying Xun and X. Sunney Xie

Science **302** (5643), 262-266.
DOI: 10.1126/science.1086911

ARTICLE TOOLS http://science.sciencemag.org/content/302/5643/262

SUPPLEMENTARY MATERIALS http://science.sciencemag.org/content/suppl/2003/10/09/302.5643.262.DC1

RELATED CONTENT http://science.sciencemag.org/content/sci/302/5643/239.full

REFERENCES This article cites 37 articles, 17 of which you can access for free
http://science.sciencemag.org/content/302/5643/262#BIBL

PERMISSIONS http://www.sciencemag.org/help/reprints-and-permissions

Use of this article is subject to the Terms of Service

Science (print ISSN 0036-8075; online ISSN 1095-9203) is published by the American Association for the Advancement of Science, 1200 New York Avenue NW, Washington, DC 20005. 2017 © The Authors, some rights reserved; exclusive licensee American Association for the Advancement of Science. No claim to original U.S. Government Works. The title *Science* is a registered trademark of AAAS.

Downloaded from http://science.sciencemag.org/ on January 4, 2018